

JGR Space Physics

RESEARCH ARTICLE

10.1029/2025JA033817

Key Points:

- A structured parallel electric field is observed in a magnetosheath reconnecting current sheet
- A parallel electric field is observed concurrent with bidirectional beams, increased electron pressure, and temperature anisotropy
- The parallel electric field accelerates and traps electrons, causing flat-top electron distributions and significant electron heating

Correspondence to:

R. Wang,
rswan@ustc.edu.cn








Citation:

Wang, S., Wang, R., Lu, Q., Huang, K., Lu, S., Shu, Y., & Guo, J. (2025). Electron acceleration by structured parallel electric field within a reconnecting current sheet in the turbulent magnetosheath. *Journal of Geophysical Research: Space Physics*, 130, e2025JA033817. <https://doi.org/10.1029/2025JA033817>

Received 4 FEB 2025

Accepted 4 SEP 2025

Electron Acceleration by Structured Parallel Electric Field Within a Reconnecting Current Sheet in the Turbulent Magnetosheath

Shimou Wang^{1,2,3} , Rongsheng Wang^{1,2,3} , Quanming Lu^{1,2,3} , Kai Huang^{4,5} , San Lu^{1,2,3} , Yukang Shu^{1,2,3} , and Jin Guo^{1,2,3} 

¹Deep Space Exploration Laboratory/School of Earth and Space Sciences, University of Science and Technology of China, Hefei, China, ²CAS Center for Excellence in Comparative Planetology/CAS Key Laboratory of Geospace Environment/Anhui Mengcheng National Geophysical Observatory, University of Science and Technology of China, Hefei, China, ³Collaborative Innovation Center of Astronautical Science and Technology, Harbin, China, ⁴School of Physics, Harbin Institute of Technology, Harbin, China, ⁵Laboratory for Space Environment and Physical Sciences, Harbin Institute of Technology, Harbin, China

Abstract Turbulent energy dissipation and the resulting plasma heating are thought to be important in various space and astrophysical systems. In this study, we present in situ evidence of electron acceleration by a localized parallel electric field in the turbulent magnetosheath, the region downstream of the Earth's bow shock. The observed profile of the parallel electric field presents a near unipolar spike, with numbers of irregular bipolar signals superimposed. This structured parallel electric field is generated in an ion-scale reconnecting current sheet, concurrent with observations of field-aligned bidirectional electron beams, large energy dissipation, and significant electron parallel heating, indicating a link between them. The electrons are demonstrated to be trapped in this current sheet and accelerated directly by a parallel electric field. Our results reveal that flat-top electron distributions, which are commonly observed in the magnetosheath, do not have to originate from the shock acceleration but can also be generated by a localized acceleration potential. Such an acceleration potential is common in reconnecting current sheets, and its contribution to electron heating can be significant in a turbulent system populated by numerous current sheets.

1. Introduction

Magnetic reconnection is a fundamental plasma process that rapidly converts magnetic energy into plasma kinetic energy and heating (Yamada et al., 2010). Thin current sheets are essential for initiating magnetic reconnection (Birn & Hesse, 2014; Liu et al., 2020; S. Lu et al., 2020). In turbulent plasma environments, thin current sheets can spontaneously form due to the non-linear energy cascade from large to small scales (Bruno & Carbone, 2013), and are considered regions where energy dissipation and plasma heating occur (Chasapis et al., 2015; Dmitruk et al., 2004; Wan et al., 2012). However, the detailed mechanisms of dissipation and heating at kinetic scales within these current sheets remain unclear.

The Earth's magnetosheath is a typical turbulent environment in near-Earth space, particularly downstream of the quasi-parallel shock, where numerous thin current sheets can be observed (Karimabadi et al., 2014; Q. M. Lu, Wang, et al., 2020; Vörös et al., 2016). Recent studies have shown that current sheets downstream of the quasi-parallel shock originate from upstream waves (Q. M. Lu et al., 2024; S. M. Wang, Lu, et al., 2024). These upstream waves are convected toward the shock by the solar wind, become compressed when transmitted through the shock, and are finally transformed into current sheets in the magnetosheath. Some simulations and observations have indicated that these current sheets are associated with magnetosheath transient structures, such as high-speed jets (E. Eriksson et al., 2016; Guo et al., 2023; Plaschke et al., 2017; S. M. Wang, Wang, et al., 2024). Magnetic reconnection signatures have been observed in these downstream magnetosheath current sheets (Chen et al., 2018; Phan et al., 2018; Retinò et al., 2007; Vörös et al., 2017; Yordanova et al., 2016), and reconnection dominates small-scale energy dissipation therein (H. S. Fu et al., 2017; Stawarz et al., 2022; Sundkvist et al., 2007; S. M. Wang, Wang, Lu, Burch, & Wang, 2021).

Recent high-resolution and three-dimensional measurements of electric and magnetic fields from the Magnetospheric Multiscale (MMS) mission (Burch, Moore, et al., 2016) have revealed new characteristics of magnetic reconnection in the magnetosheath. One striking finding is the presence of large-amplitude and spiky parallel

electric field structures that significantly influence electron dynamics (Phan et al., 2018; S. M. Wang, Wang, Lu, Russell, et al., 2021; Wetherton et al., 2022; Wilder et al., 2017). These reconnection events are typically associated with large guide fields, and analyses of multiple events in the magnetosheath show that the magnitude of the parallel electric field spikes is positively correlated with the strength of the guide fields (Wilder et al., 2018). Some of these parallel electric field spikes are not linked to the reconnection X line or separatrix region (S. Eriksson et al., 2016; S. Y. Huang et al., 2021; Mozer & Pritchett, 2010; H. W. Wang et al., 2023; R. S. Wang et al., 2014), but instead coincide with an extended electron jet (Wilder et al., 2017). The presence of such strong parallel electric field spikes can directly accelerate electrons passing through them, generating high-energy electron beams and exciting instabilities to form electron holes (S. M. Wang, Wang, Lu, Russell, et al., 2021). Nevertheless, the spatial distribution of these parallel electric field structures and their role in electron dynamics during magnetic reconnection in the magnetosheath are still not fully understood due to the limited reconnection events observed in this turbulent region.

In this study, we present in situ MMS observations of a parallel electric field event within a reconnecting current sheet in the magnetosheath. This parallel electric field generates a parallel acceleration potential of 30 V, which accelerates and traps electrons in the reconnection region. We investigate the effect of such a localized acceleration potential on energy dissipation and electron energization. The analysis uses magnetic field data from the Fluxgate Magnetometer (Russell et al., 2016), electric field data from the Electric Double Probes (Ergun, Tucker, et al., 2016; Lindqvist et al., 2016), and electron and ion data from the Fast Plasma Investigation (Pollock et al., 2016).

2. Event Overview

Figure 1 provides an overview of the crossing of the MMS1 spacecraft from the solar wind to the quasi-perpendicular magnetosheath, and finally to the quasi-parallel magnetosheath, between 10:00 and 13:00 UT on 16 February 2022. The position of MMS1 in the Geocentric Solar Ecliptic (GSE) coordinate system is shown at the bottom of Figure 1, indicating that MMS1 was slowly moving toward the Earth (~ 2 km/s) along the X direction. The blue and orange vertical dashed lines in Figure 1 represent the encounters with the bow shock and the boundary between the quasi-perpendicular and quasi-parallel magnetosheath, respectively. Initially, MMS1 was in the solar wind, characterized by a narrow ion spectrogram (Figure 1a), low magnetic field strength (Figure 1c), low density (Figure 1d), and a large anti-sunward ion flow (Figure 1e). After about 10:39 UT (marked by the blue vertical dashed line), MMS1 crossed the bow shock and entered the magnetosheath, which was populated by the shocked solar wind. After the shock, the plasma flow deviated from the pristine $-X_{\text{GSE}}$ direction to $(-X, +Y, -Z)_{\text{GSE}}$ direction, consistent with the expected behavior of magnetosheath plasma flowing around the Earth's magnetosphere.

The magnetosheath interval in Figure 1 is divided into two subregions: the quasi-perpendicular magnetosheath and the quasi-parallel magnetosheath, each with distinct properties. The quasi-perpendicular magnetosheath (before the orange vertical dashed line) has broader ion and electron spectrograms, higher density, and larger thermal pressure (Figure 1f). In contrast, the quasi-parallel magnetosheath (after the orange vertical dashed line) exhibits stronger fluctuations in the magnetic field, density, and ion flow, indicating a more turbulent state. High-energy ions with energies larger than 10 keV are detected in the quasi-parallel magnetosheath, suggesting significant ion heating and acceleration. The total pressure (the sum of magnetic pressure and plasma thermal pressure) in the quasi-parallel magnetosheath interval is generally lower than that in the quasi-perpendicular magnetosheath. These differences in properties between the two subintervals are caused by the change in the direction of the upstream solar wind magnetic field, which is also reflected in the overall profile of the observed magnetosheath magnetic field.

Figure 1g shows the current density calculated using the curlometer method (Dunlop et al., 2002). The current density in the quasi-parallel magnetosheath increases substantially, exhibiting some localized spikes. The amplitude of these current density spikes can reach $1.2 \mu\text{A}/\text{m}^2$, comparable to typical current density values observed in magnetopause reconnection events (Burch, Torbert, et al., 2016; R. S. Wang et al., 2017). These large current spikes correspond to thin current sheets where magnetic reconnection could potentially occur. In contrast, the current density in the quasi-perpendicular magnetosheath is much smaller, typically less than $0.3 \mu\text{A}/\text{m}^2$, and there are no reconnection events found. Next, we mainly focus on the thin current sheet denoted by the blue arrow in Figure 1g.

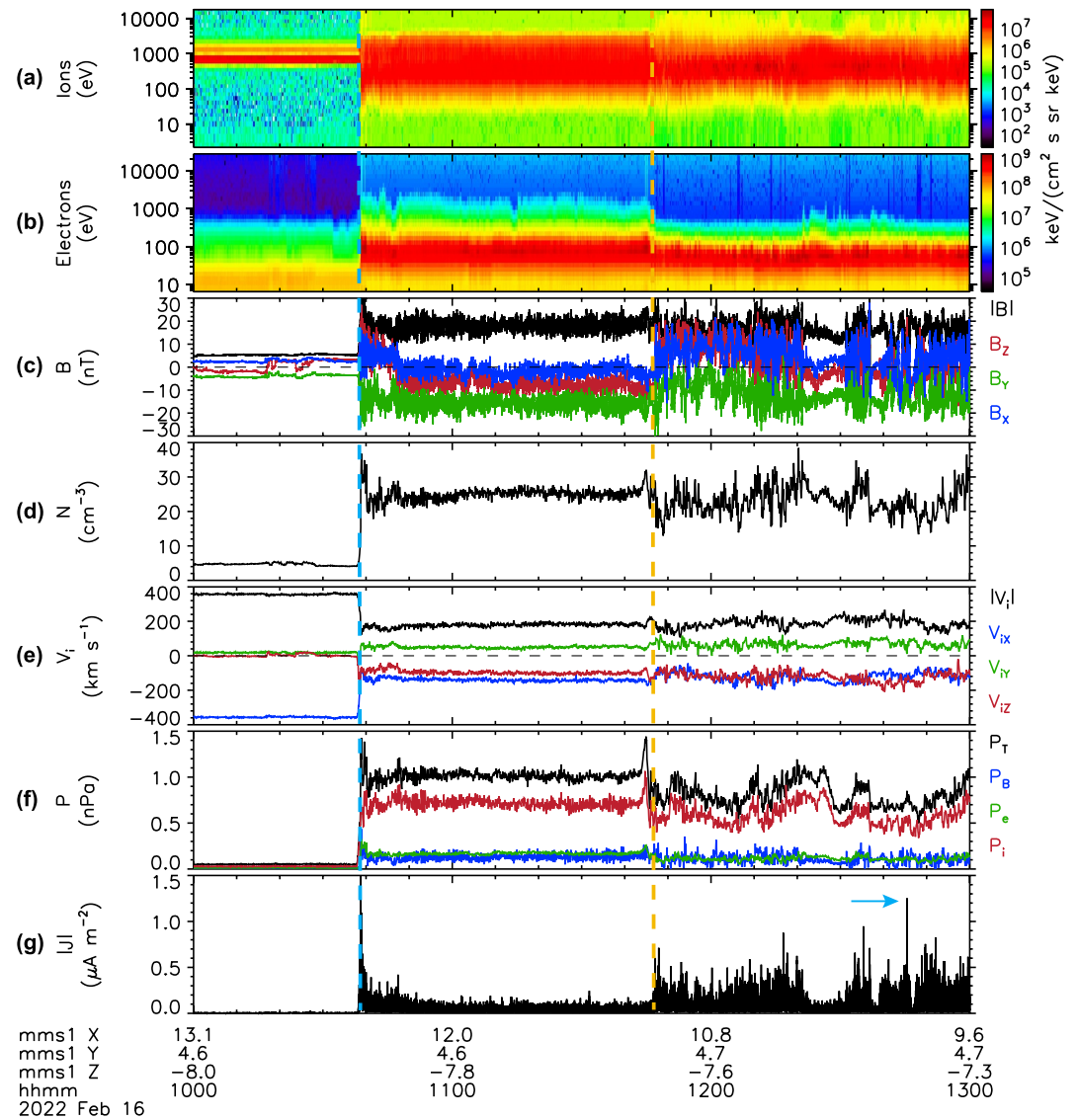


Figure 1. Overview of the MMS1 observations in the magnetosheath. (a) Ion differential energy flux. (b) Electron differential energy flux. (c) Magnetic field. (d) Electron density. (e) Ion bulk velocity. (f) Total, magnetic, electron, and ion pressures. (g) Total current density. The data are displayed in Geocentric Solar Ecliptic (GSE) coordinate system.

3. Reconnection Signatures in the Current Sheet

Figure 2 shows the MMS1 observations surrounding the current sheet from 12:45:20 to 12:45:35 UT. To identify the reconnection signatures in this current sheet, the spacecraft data are transformed into a current sheet boundary normal (LMN) coordinate system, where L is along the reconnecting magnetic field direction, N is along the current sheet normal, and $M = N \times L$ is the direction out of the reconnection plane. The LMN coordinate system is obtained by minimum variance analysis (Sonnerup & Cahill, 1967) applied to the magnetic field data over the interval from 12:45:27.5 to 12:45:28.0 UT. Relative to the GSE coordinate system, $L = (-0.40, 0.62, 0.67)$, $M = (-0.09, -0.76, 0.64)$, and $N = (0.91, 0.20, 0.36)$. The four-spacecraft timing method indicates that the current sheet moved with a speed of 138 km/s along the $-N$ direction. The background plasma velocity along the $-N$ direction is approximately 150 km/s, with the velocity at the trailing edge of the current sheet being larger than at the leading edge. Therefore, the current sheet was being compressed by the background bulk flow when the spacecraft crossed it.

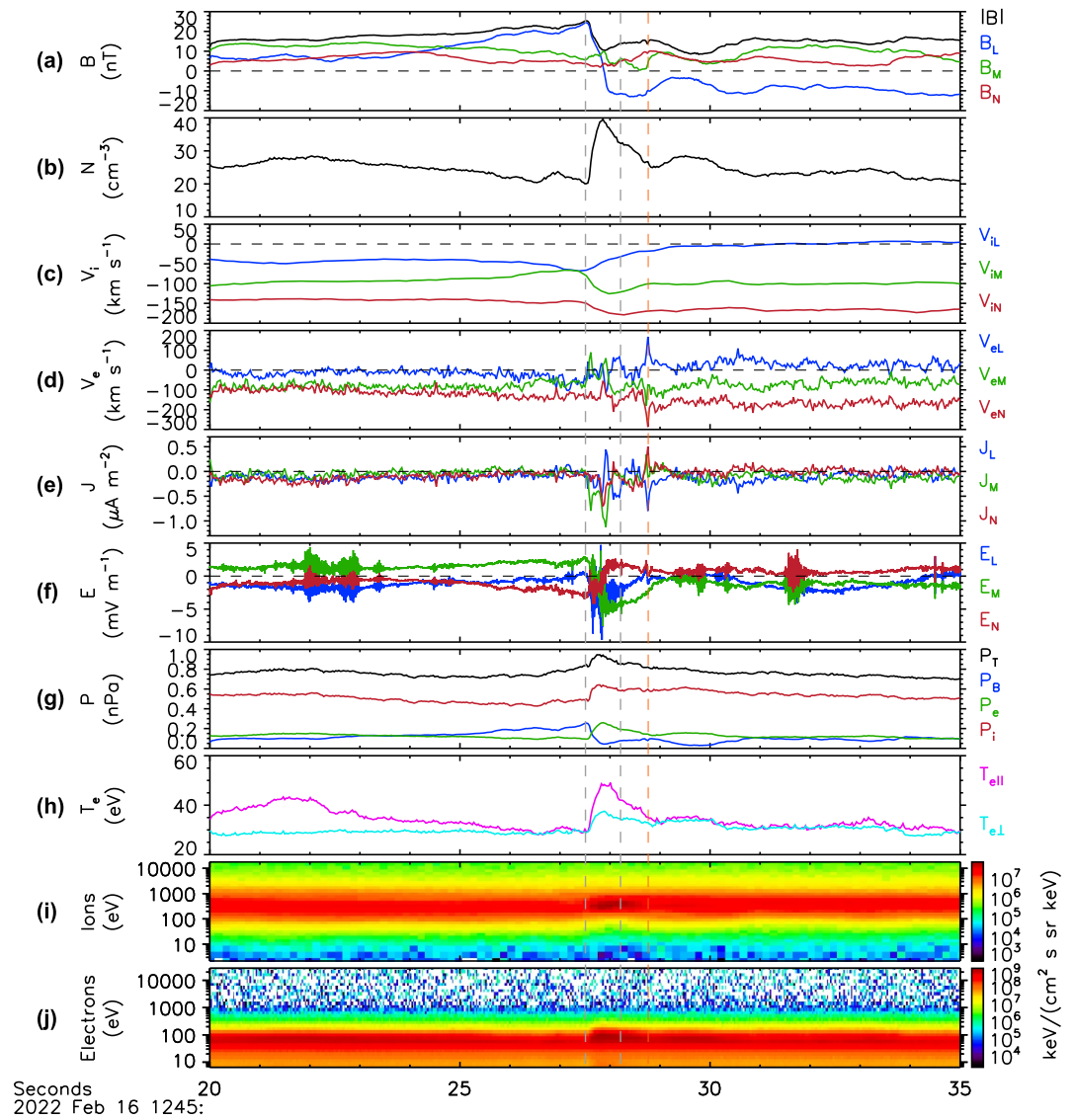


Figure 2. Enlarged view of the current sheet observed by MMS1. (a) Magnetic field. (b) Electron density. (c) Ion bulk velocity. (d) Electron bulk velocity. (e) Current density. (f) Electric field. (g) Total, magnetic, electron, and ion pressures. (h) Electron parallel and perpendicular temperatures. (i) Ion differential energy flux. (j) Electron differential energy flux. The data are displayed in a current sheet boundary normal (*LMN*) coordinate system. Relative to the GSE coordinate system, $\mathbf{L} = (-0.40, 0.62, 0.67)$, $\mathbf{M} = (-0.09, -0.76, 0.64)$, and $\mathbf{N} = (0.91, 0.20, 0.36)$.

The crossing of the current sheet is clearly identified by a reversal of the reconnecting magnetic field component B_L (Figure 2a), from ~ 25 nT to ~ -12 nT, between the two gray vertical dashed lines, which corresponds to a negative current J_M spike up to $-1.1 \mu\text{A}/\text{m}^2$ (Figure 2e). Here, the current density is calculated using the plasma moments data. The out-of-plane magnetic field component B_M right outside the current sheet, which is usually referred to as the guide field B_g , is approximately 6 nT. After subtracting the guide field, B_M exhibits a bipolar variation from positive to negative, consistent with the Hall magnetic field signal on one side of the X-line. After the second gray vertical dashed line, MMS1 observed another negative B_M variation that persists for 0.8 s, together with a nearly constant negative B_L value (-12 nT), indicating that the spacecraft remained within the current sheet. A possible spacecraft trajectory passing through the current sheet is shown by the black dashed arrow in Figure 3. The magnetic field strength increases at both edges of the current sheet, implying magnetic field pileup (Øieroset et al., 2019). In contrast, the magnetic field strength has a dip at the reversal point of B_L . The electron density (Figure 2b) exhibits an anti-correlated variation with magnetic field strength throughout the

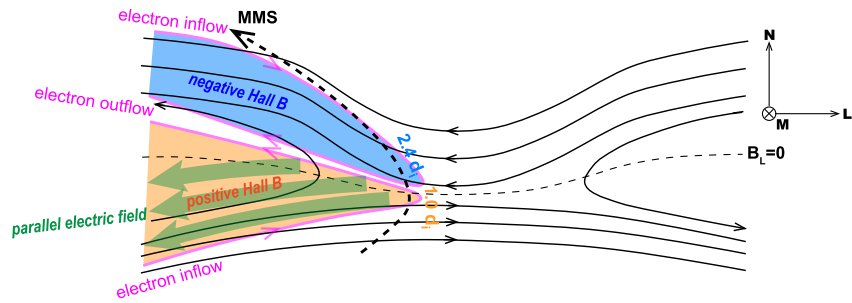


Figure 3. A sketch of the reconnecting current sheet in the L - N plane. The trajectory of the MMS spacecraft through the current sheet is denoted by the black dashed arrow. The blue and orange shaded regions represent two quadrants of the Hall magnetic field region, with corresponding Hall electron current system shown by magenta curves. The green arrows indicate the parallel electric field pointing outward from the X line.

interval and has a peak of 40 cm^{-3} at the center of the current sheet. Note that the electron density shows a local dip at the site where MMS1 entered or exited the current sheet.

From the ion bulk velocity shown in Figure 2c, the ion velocity V_{iL} outside the current sheet varies from -50 km/s to 0 km/s at two sides, suggesting that the current sheet is embedded in a background shear flow. Additionally, V_{iL} shows a local dip down to -70 km/s near the leading edge of the current sheet (the first vertical dashed line), which probably corresponds to negative reconnection outflow. The deviation of the maximum outflow velocity from the center of the current sheet could be attributed to asymmetric magnetic field and plasma conditions (Shay et al., 2016). The out-of-plane ion flow V_{iM} in the current sheet shows an increase followed by a decrease after subtracting the background flow (-100 km/s). The V_{iM} increase is closely associated with the negative reconnection outflow that is located at the edge of the current sheet, while the V_{iM} decrease is observed inside the current sheet (between the two gray vertical dashed lines). Beyond the same variation to the ion flow at the leading edge of the current sheet, including a dip in V_{eL} and an increase in V_{eM} , the electron flow shows more structured narrow bursts compared to the ion flow (Figure 2d). Between the two gray vertical dashed lines, V_{eL} exhibits two peaks with a dip between them, leading to a corresponding J_L variation from negative to positive to negative (Figure 2e). This kind of J_L variation is in good agreement with the Hall electron current system on the negative outflow side (as illustrated in Figure 3) in collisionless magnetic reconnection and generates the observed Hall magnetic field. Additionally, V_{eM} and J_M each present two isolated peaks, suggesting that the current sheet has a bifurcated structure. The negative V_{iM} enhancement, along with the positive V_{eM} enhancement inside the current sheet, suggests that they are accelerated by the negative E_M up to -5 mV/m (Figure 2f). Simultaneously, MMS1 observed $+N$ and $-N$ directional electron inflows after subtracting the convection velocity of the current sheet. The electron inflow velocity is about 70 km/s . A striking feature is that all three components of electron velocity and the corresponding current density exhibit localized bursts at the orange vertical dashed line. This narrow current layer has a positive J_M value, opposite to that in the main current sheet, implying that this variation is not due to the spacecraft returning to the current sheet. We note that this narrow current structure is associated with the variation of magnetic field component B_M and a dip of magnetic field strength. We speculate that this narrow current structure may be related to the three-dimensional reconnection separatrix region (Bai et al., 2019, 2025; Daughton et al., 2011; X. S. Fu et al., 2024).

Figure 2g shows different plasma pressures. The total pressure (sum of magnetic and thermal pressure) outside the current sheet is nearly constant ($\sim 0.75 \text{ nPa}$) and smaller than that within the current sheet ($\sim 0.95 \text{ nPa}$), indicating that the current sheet is not in pressure balance and has a tendency to expand. The pressure imbalance is primarily due to changes in plasma thermal pressure associated with variations in number density and temperature. For electrons, both the parallel and perpendicular temperatures increase significantly compared to the background magnetosheath, indicating substantial electron heating. This is also evident in the omnidirectional electron energy spectrogram (Figure 2j), which shows a broadening of the distribution within the current sheet. In contrast, the ion energy spectrogram (Figure 2i) shows a local narrowing but with enhancements in fluxes around 400 eV . We note that the electron temperature anisotropy begins to arise from the first gray vertical dashed line, where a density dip is observed, which is consistent with MMS1 crossing the reconnection separatrix. It is also clear that MMS1

exited the exhaust region at the orange vertical dashed line, where narrow bursts of electron flows and electric fields vanish. Therefore, the width of the exhaust region is 165.6 km, ~ 3.4 ion inertial lengths.

Based on the observations in Figure 2 including weak reconnection outflow, simultaneous electron flows in the $\pm L$ and $\pm N$ directions, Hall magnetic field, and electron heating, we conclude that reconnection was occurring in this magnetosheath current sheet, and MMS1 crossed the ion diffusion region and was in close proximity to the electron diffusion region.

4. Structured Parallel Electric Field in the Diffusion Region

In Figure 4, we examine the current and electric field within the current sheet, which are essential for energy conversion and electron acceleration. The Hall magnetic field B_M and corresponding Hall current system J_L are clearly seen in Figures 4a and 4c between the first and third vertical dashed lines. The horizontal purple dashed line in Figure 4a represents the background guide field (~ 6 nT). The negative V_{eN} jet together with $+N$ to $-N$ variation in V_{eN} around the second vertical dashed line suggests that the spacecraft was near or crossing the electron diffusion region during this short interval (from 12:45:27.8 to 12:45:28.05 UT). The electron inflow velocity calculated from bipolar V_{eN} variation (Pritchard et al., 2019) is 75 km/s, about $0.03 V_{AeL}$, implying a reconnection rate of 0.03 (Burch et al., 2020). At the same time, J_M reaches its maximum value ($-1.0 \mu\text{A}/\text{m}^2$) and is primarily antiparallel to the magnetic field (Figure 4d). J_M shows another peak at the leading edge of the current sheet ($\sim 12:45:27.6$ UT), where the current is nearly perpendicular to the magnetic field. This current peak, located near the edge of the current sheet, is likely caused by local magnetic field pileup.

Figures 4e–4g present the three components of $-(\mathbf{V}_e \times \mathbf{B})$, $-(\mathbf{V}_i \times \mathbf{B})$, and the measured perpendicular electric field with its error, respectively. In the possible electron diffusion region from 12:45:27.8 to 12:45:28.05 UT, there is a significant deviation between $-(\mathbf{V}_e \times \mathbf{B})$ and \mathbf{E}_\perp , especially in the L and M direction, indicating that electrons are demagnetized therein. Here, we use the maximum E_M as the reconnection electric field. After subtracting high-frequency electric field fluctuations, the reconnection electric field is about 4.6 mV/m, consistent with the typical value in magnetosheath reconnection (Phan et al., 2018). The normalized reconnection rate is calculated by $\frac{E_M}{V_{AeL} B_L}$ (Burch et al., 2020), where V_{AeL} is the electron Alfvén speed, and B_L is the L component of the magnetic field in asymmetric reconnection. The use of V_{AeL} here is appropriate by the fact that near the electron diffusion region the magnetic field is advected by the electrons (Burch et al., 2020). Using this method, the reconnection rate is determined as ~ 0.09 , slightly larger than that derived from electron inflow speeds. A reconnection rate near 0.1 is common in observations and simulations (Burch et al., 2020; Liu et al., 2017; Q. Lu et al., 2025; Pritchard et al., 2023), indicating efficient energy conversion. Figure 4h shows the parallel electric field E_\parallel . A predominantly negative E_\parallel with strong fluctuations is observed just inside the positive Hall magnetic field region (between the first and second vertical dashed lines), coincident with increased plasma density (Figure 4b). The E_\parallel exhibits two peaks with amplitude exceeding 10 mV/m and is primarily from the electric field component E_L (Figure 4i) that points away from the X line as indicated by the green arrows in Figure 3. This structured E_\parallel causes significant energy dissipation $\mathbf{J} \cdot \mathbf{E}'$, with a maximum value of up to $4 \text{ nW}/\text{m}^3$. In contrast, the value of E_\parallel in the negative Hall magnetic field region is overall positive ($\sim 1 \text{ mV}/\text{m}$) but is smaller than the uncertainty of measurement. Thus, it is unclear whether this small E_\parallel is real.

On the other hand, strong waves are observed in two E_\parallel peaks (Figures 4i, 4j, 4l, and 4m) with amplitudes comparable to the negative parallel electric field peaks. These waves are primarily parallel to the magnetic field (Figures 4i and 4j). In the first peak, the waves are in the L direction, whereas in the second peak, they exhibit L and M directional components. The Hall electric field E_N is dominated by a DC component.

Figures 4l and 4m show the electric and magnetic field power spectral densities, respectively. Significant electric field power enhancements occur from ~ 300 Hz to ~ 2 kHz in the first E_\parallel peak and from ~ 100 Hz to ~ 1 kHz in the second peak. The wave frequency exceeds the electron cyclotron frequency f_{ce} (white line) and extends up to the ion plasma frequency f_{pi} (magenta line). Crucially, no corresponding enhancements appear in the magnetic field power, indicating that these waves are electrostatic. Such parallel, electrostatic, ion plasma frequency waves have been documented in the diffusion region of magnetopause reconnection (Ergun, Holmes, et al., 2016; Steinvall et al., 2021; Wilder et al., 2016; Zhong et al., 2021), although the amplitude in our event is smaller. Close examination of parallel electric field waveforms reveals these electrostatic waves superimposed on a negative DC parallel electric field, exhibiting nonlinear evolution at different times. After subtracting the DC component, these

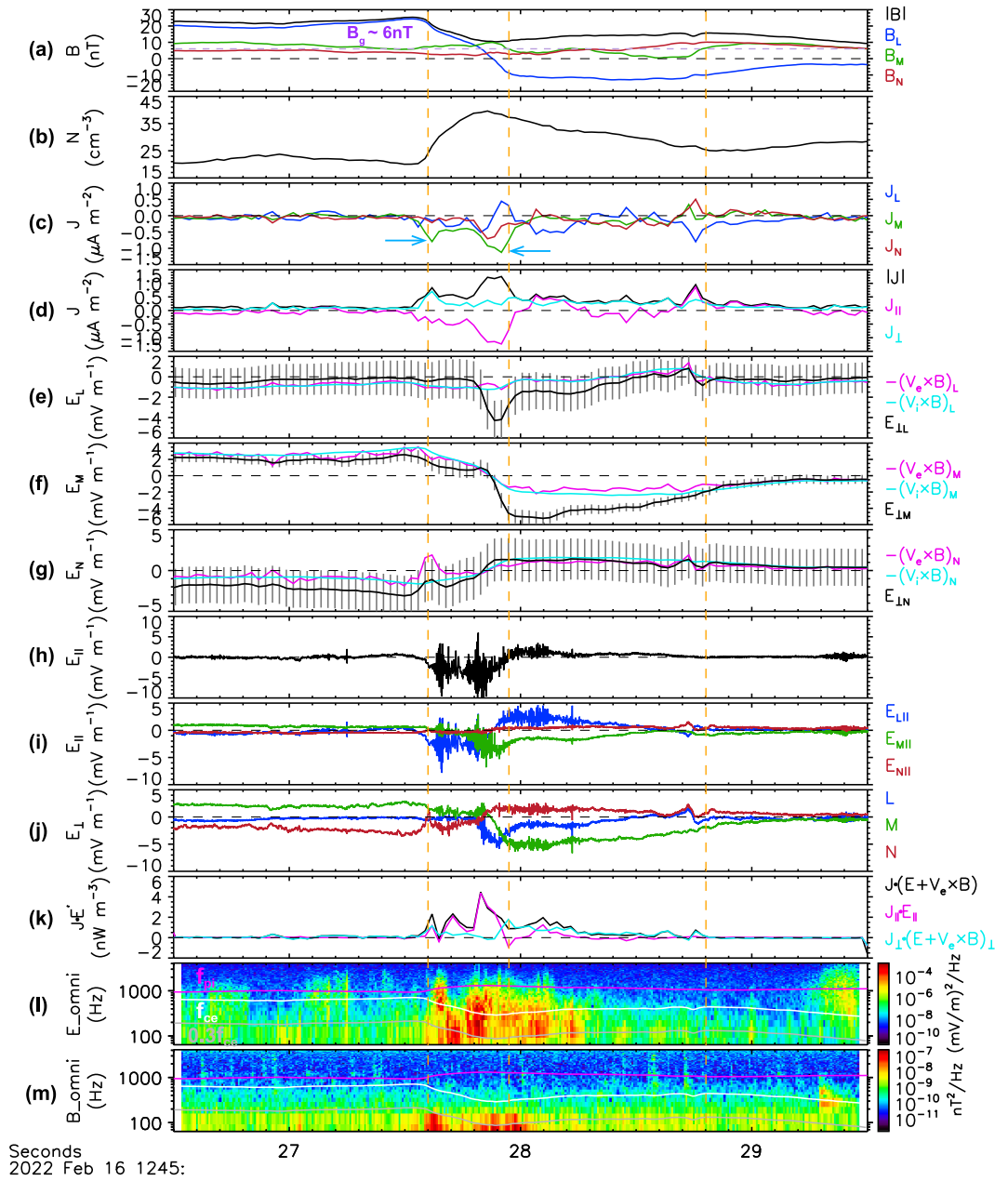


Figure 4. Current and electric field within the current sheet. (a) Magnetic field. (b) Electron density. (c) Current density. (d) Total current density and its parallel and perpendicular components. (e–g) L , M , and N components of $-(\mathbf{V}_e \times \mathbf{B})$, $-(\mathbf{V}_i \times \mathbf{B})$ and perpendicular electric field, respectively. (h) Parallel electric field. (i) Parallel components of the electric field E_L , E_M , and E_N . (j) Perpendicular electric field. (k) Energy dissipation $\mathbf{J} \cdot \mathbf{E}' = \mathbf{J} \cdot (\mathbf{E} + \mathbf{V}_e \times \mathbf{B})$ and its contribution from parallel and perpendicular current and electric field. (l) Electric field power spectral density. (m) Magnetic field power spectral density.

waves display bipolar or continuous steepening waveforms, similar to those reported in the magnetotail diffusion region by Yu et al. (2021). Notably, the positive wave electric fields exceed the negative amplitudes, which suggests that the net potential associated with these waves impedes electron inflow toward the reconnection region. Additionally, electromagnetic waves with enhanced power near $0.3 f_{ce}$ (gray line) appear in the two E_{\parallel} peaks. Wave polarization analysis indicates right-hand circular polarization and oblique propagation, consistent with whistler wave characteristics.

Simultaneous observations of electrostatic and whistler waves are not rare in magnetic reconnection (Wilder et al., 2019). These waves can affect the reconnection process, such as electron heating, anomalous resistivity, and pitch-angle scattering (Graham et al., 2025). In our event, the net potential associated with the electrostatic waves seems to prevent electrons from flowing into the reconnection region. However, as demonstrated below, electron dynamics in our event are dominated by the negative E_{\parallel} peaks, rather than these wave activities.

The large-amplitude, outward-pointing E_{\parallel} is detected by all four MMS satellites. Figure 5a plots the magnetic field component B_L for the four satellites. The current sheet, with B_L varying from positive to negative, was sequentially crossed by MMS2/3/1/4, in an order consistent with their locations in the N direction (Figures 5i and 5j). Note that when MMS4 entered into the current sheet, MMS2 left the current sheet. This suggests that four MMS satellites cannot be inside the current sheet simultaneously. Therefore, the linear approximation was not satisfied in our event, and multi-spacecraft analysis, such as the minimum directional derivative (MDD) method (Shi et al., 2005) and spatial-temporal difference (STD) method (Shi et al., 2006), was not applicable in our event. The negative-to-positive Hall magnetic field signatures, superposed on the guide field observed by all four satellites, are shown in Figure 5b. The vertical dashed lines denote the boundary separating the positive and negative Hall magnetic field regions. After MMS2/3/4 observations are time shifted to be aligned with the MMS1 observation of $B_L = 0$ (Figures 5c and 5d), we note that the four satellites entered the current sheet at different times (MMS1/4/3/2) but exited almost simultaneously. This suggests different current sheet widths and/or compression at the four satellites. The compression occurs at the leading edge (earthward side) of the current sheet and is the strongest at MMS2.

Figures 5e–5h show the parallel electric fields for the four satellites, respectively. Negative and fluctuating E_{\parallel} signals are clearly found at all four satellites and are located in the positive Hall magnetic field region (before the corresponding vertical dashed lines). We note that the amplitude of E_{\parallel} is not correlated with the distance to the X line (the locations of four satellites in the L direction). This implies the characteristic scale of this E_{\parallel} structure should be larger than the separation of satellites along the L direction (~ 30 km, 0.6 ion inertial lengths). Given the width of the positive Hall magnetic field region along the N direction, this E_{\parallel} structure covers a volume of at least $0.6d_i \times 1.0d_i$ ($L \times N$) in the reconnection plane. Such an outward-pointing and unipolar E_{\parallel} structure is rarely reported in previous observations of reconnecting current sheets.

5. The Effect of Parallel Electric Field on Electron Dynamics

It is natural to expect that this widely distributed and orientated E_{\parallel} can accelerate electrons to stream toward the reconnection site and cause trapping of electrons. From Figure 6c, we see an evident increase in electron pressure in the L and N directions, concurrent with the presence of E_{\parallel} structure in Figure 6b. Figures 6d–6f show the electron pitch angle distributions (PADs) in the energy ranges 6–100 eV, 100–400 eV, and 400–2000 eV, respectively. The electron fluxes around 0° and 180° pitch angles begin to increase substantially (Figures 6d and 6e) after $\sim 12:45:27.6$ UT (the first vertical dashed line), and this enhancement persists in the positive Hall magnetic field region, coincident with the E_{\parallel} structure (Figure 6b). Therefore, the edge of the positive Hall magnetic field (the first vertical dashed line) corresponds to the location of the separatrix, where inflowing electrons are streaming along 0° pitch angle toward the X line. This kind of bidirectional distribution fades in the negative Hall magnetic field region, where more electrons concentrate at 180° pitch angle, corresponding to inflowing electrons along the upper separatrix region in Figure 3. The correlation between the bidirectional electron PADs and the outward-pointing E_{\parallel} indicates that E_{\parallel} can trap electrons in the ion diffusion region. We note that the electrons from 400 to 2000 eV are more isotropic, although their fluxes are also higher than the background (Figure 6f). This implies that some processes lead to the isotropy of these higher-energy electrons.

To investigate the acceleration effect of E_{\parallel} on electrons, we plot the electron phase space density (PSD) versus energy E , observed outside (12:45:20.0 UT and 12:45:35.0 UT) and inside (12:45:27.8 UT) the current sheet, in Figure 7. The electron anisotropy within the current sheet is clearly seen in Figure 7a, where the PSD in the parallel and antiparallel directions is almost the same and substantially larger than that in the perpendicular direction, which corresponds to the acceleration of electrons parallel to the magnetic field in the diffusion region. Furthermore, the accelerated electrons exhibit a flat-top distribution from 30 eV up to 70 eV, typical for electron distributions in reconnection (Asano et al., 2008).

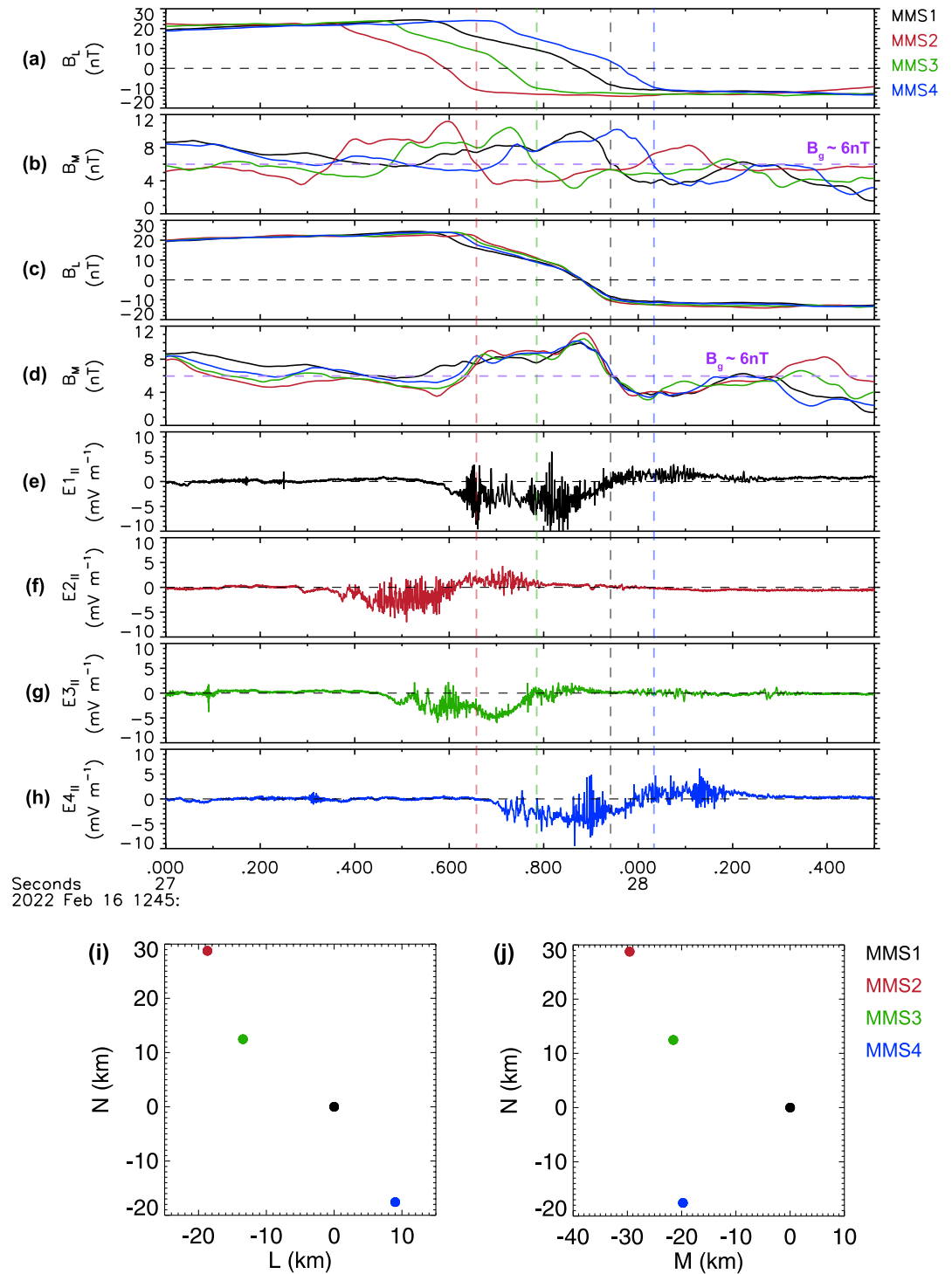


Figure 5. Observations of the current sheet from the four MMS spacecraft. (a) Magnetic field component B_L . (b) Magnetic field component B_M . (c and d) Magnetic field components B_L and B_M , with MMS2/3/4 observations time shifted to be aligned with the MMS1 observation of $B_L = 0$. (e)–(h) Parallel electric fields from the four MMS spacecraft, respectively. (i and j) Relative positions of the four MMS spacecraft in the L - N and M - N planes.

To test whether the acceleration by $\phi_{||}$ is consistent with the measured electron distributions, we consider the results in Figures 7b and 7c, where the blue and red dot lines show the background electron distributions from two sides of the current sheet, and the green dot line is the accelerated electron distribution within the diffusion region.

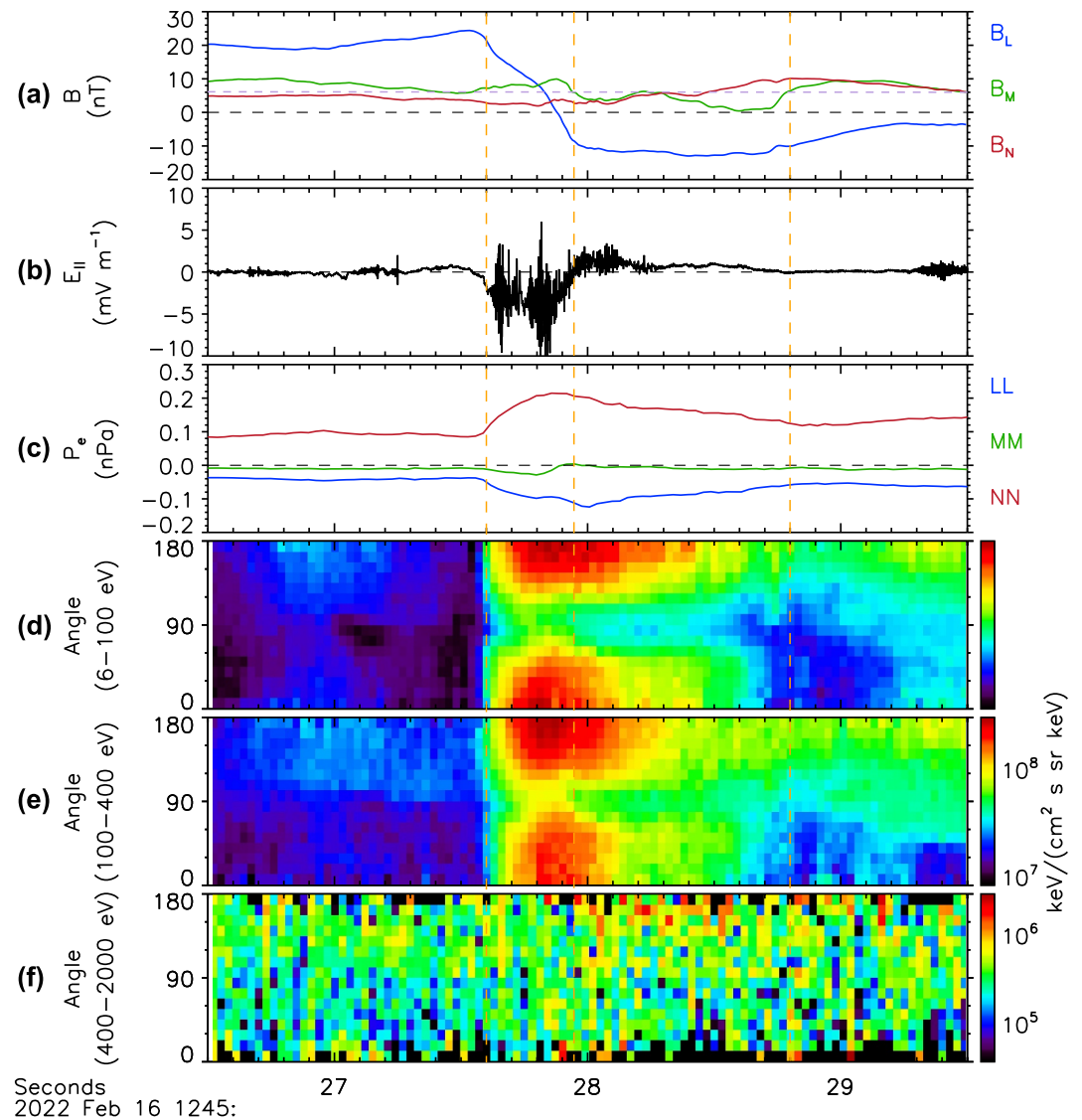


Figure 6. Electron data observed by MMS1 within the current sheet. (a) Magnetic field. (b) Parallel electric field. (c) Diagonal terms of the electron pressure tensor. (d–f) Pitch angle distributions of electrons in the energy range of 6–100 eV, 100–400 eV, and 400–2000 eV, respectively.

The flat-top distribution is also observed for the background electrons, which has been found to be common for magnetosheath electrons (Feldman et al., 1983; Graham et al., 2021) and is attributed to acceleration by a cross-shock potential (Feldman et al., 1983; Scudder, 1995). The increase of the maximum flat-top electron energy from 40 eV for the background electrons to 70 eV for the energized electrons in the reconnection region is clearly visible. Using Liouville's theorem by assuming $df/dt = 0$ along the electron trajectory, we map the accelerated electrons with a potential $\phi_{||}$ of 30 V (black dots in Figure 7b), which agrees well with the observed distribution in the reconnection region (green dot line in Figure 7b). The distribution $f_{||}$ at 12:45:20.0 UT is used as the background. The electron acceleration by $\phi_{||}$ is evidenced by large PSD values with energy larger than 40 eV. The energy gain of the electrons (<300 eV) based on the Liouville mapping is nearly independent of energy, which is a typical signature of energization by an acceleration potential (Egedal et al., 2010). The PSD of electrons >300 eV is significantly larger than that of the mapped electrons, which implies that these higher-energy electrons are likely further accelerated by other mechanisms. Some processes should be involved to scatter these higher-energy electrons to isotropic distributions, as seen in Figure 6f. The acceleration potential obtained from the parallel and

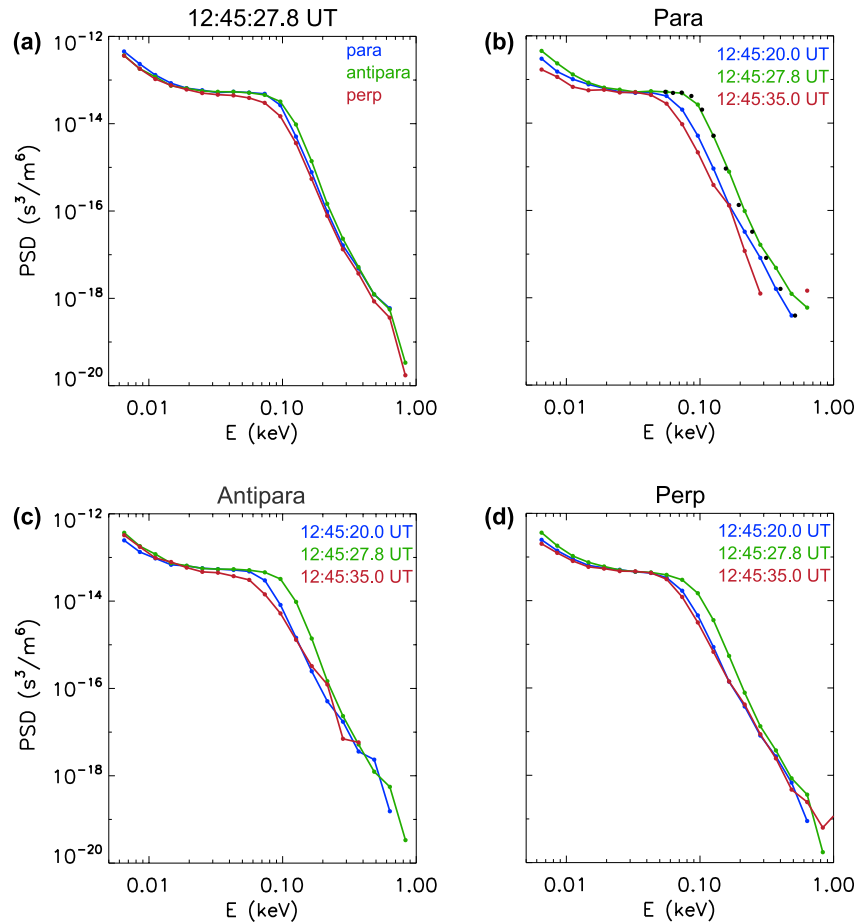


Figure 7. Electron distribution function observed by MMS1. (a) Electron distributions in parallel, antiparallel, and perpendicular directions at 12:45:27.8 UT. (b) Electron distributions in parallel direction at 12:45:20.0, 12:45:27.8, and 12:45:35.0 UT. (c) Electron distributions in antiparallel direction at 12:45:20.0, 12:45:27.8, and 12:45:35.0 UT. (d) Electron distributions in perpendicular direction at 12:45:20.0, 12:45:27.8, and 12:45:35.0 UT.

antiparallel directional PSD is almost identical to Figures 7b and 7c. This also demonstrates that these accelerated electrons are trapped in the reconnection region and generate the bidirectional electron beams seen in Figures 6d and 6e. The flat-top distribution in the perpendicular direction is less prominent, but the increase in PSD indicated by the green dot lines between 50 and 300 eV is also significant (Figure 7d).

Flat-top electron distributions are also observed in turbulent reconnection regions in Earth's magnetotail (Ergun et al., 2020a, 2020b; Li et al., 2022). In these observations, a flat-top distribution appears in the parallel direction, while a nonthermal tail distribution is significant in the perpendicular direction. Ergun et al. (2020a) proposed that a flat-top distribution forms when electrons encounter a series of random parallel electric field structures in a turbulent region and then gain energy from accelerating potentials and lose energy in decelerating potentials. Since low-energy electrons are reflected by a decelerating potential without losing energy, they experience only an acceleration process before their energy reaches a critical value. In such a turbulent environment, electrons gain energy and naturally form a flat-top distribution. However, since electrons with high parallel velocity easily pass through the turbulent acceleration region, the parallel energization is limited. From this perspective, the current sheet in our event can also be regarded as an accelerator that accelerates electrons into it via a positive potential, although its scale is much smaller than that described in Ergun et al. (2020a). However, there are several key differences.

First, the magnetotail current sheet in Ergun et al. (2020a) evolved into a turbulent state and covered a large-scale region ($\sim 16 R_E$), far exceeding the scale in our event. Its complex electric field distribution and numerous random

potential structures trap electrons and cause large parallel thermal heating. In such a turbulent reconnecting current sheet, a net parallel potential at its boundary that accelerates electrons into it is not necessary to produce flat-top electron distributions. On the other hand, Ergun et al. (2020a) found that electrons with high parallel speeds become non-adiabatic and are significantly energized by large-amplitude turbulent electric fields in the perpendicular direction. Furthermore, turbulence in the magnetotail generates magnetic depletions that can trap electrons, increasing their dwell time in regions of strong electric fields. This substantially enhances perpendicular energization and produces nonthermal tail distributions. Such a perpendicular energization process and nonthermal tail distribution are not observed in our event. The primary reason is likely that magnetic trapping via the mirror force was small in our event due to the strong guide field. Additionally, the small scale of the current sheet and high plasma density in the magnetosheath limit the energy gained per particle (Qi et al., 2024).

6. Discussion and Conclusions

Parallel electric fields have been extensively studied in the diffusion region of magnetic reconnection and are crucial for energy conversion and electron acceleration during the reconnection process (Dahlin et al., 2016; Drake et al., 2005; Egedal et al., 2015; Fox et al., 2018; C. Huang et al., 2010; S. Wang et al., 2018). The distribution of these fields in reconnection is primarily controlled by the guide field and the asymmetry of the current sheet and is influenced by various instabilities (Drake et al., 2003; Lapenta et al., 2010; Pritchett, 2001; Pritchett & Coroniti, 2004). In general, the parallel electric field is directed away from the X line, accelerating inflowing electrons along the magnetic field lines. However, direct spacecraft observations of such fields remain rare. Using data from the Polar spacecraft at the magnetopause, Mozer and Pritchett (2010) reported unipolar parallel electric fields on the magnetosphere side, with directions consistent with simulations. The magnitudes of these fields were significantly larger than those predicted by the simulations. In the magnetotail, similar parallel electric field structures are observed in the separatrix, where they accelerate inflowing electrons to energies of up to 100 keV (R. S. Wang et al., 2013, 2014).

In our event, however, the parallel electric field exhibits several different features from previous studies. First, the parallel electric field pointing outward from the X line is observed in conjunction with the lower quadrant of the Hall magnetic field (Figure 3). This parallel electric field is closely associated with an electron density increase, rather than a density cavity, suggesting that it is not the same as the double layer electric fields observed in the separatrix (Mozer & Pritchett, 2010; R. S. Wang et al., 2013). In the upper quadrant of the Hall magnetic field region, the magnitude of the parallel electric field is relatively small (around 1 mV/m), falling within the uncertainty of the electric field measurements. However, its direction points toward the X line, consistent with relevant simulations (S. Lu et al., 2021). Second, the parallel electric field in our event covers a region of at least $0.6d_i \times 1.0d_i$ ($L \times N$) in the reconnection plane. Given that the parallel electric fields are observed by all four MMS spacecraft and their magnitudes are nearly identical, the spatial extent of the parallel electric field in the L direction must be greater than $0.6 d_i$. Third, the observed parallel electric field is primarily from the electric field component E_L , rather than the out-of-plane component E_M , which is typically responsible for large-amplitude parallel electric fields in previous magnetosheath reconnection events (Phan et al., 2018; S. M. Wang, Wang, Lu, Russell, et al., 2021; Wilder et al., 2017). This suggests that the parallel electric field in our event is possibly predominantly electrostatic, which is caused by charge separation (S. Lu et al., 2021). Finally, the parallel electric field appears to be structured, presenting an overall unipolar profile with many irregular bipolar parallel electric fields superimposed, which may correspond to the early stage of electron hole formation (Yu et al., 2021). This indicates that the electron beams generated by this parallel electric field structure could drive two-stream or beam instabilities that excite electron holes (Chang et al., 2022; Newman et al., 2001). However, a typical electron hole signature is not observed in this reconnection event, possibly due to the spacecraft trajectory or the different evolution stage of the instability.

Although direct observations of parallel electric fields are rare, likely due to their small magnitudes, they can generate a considerable parallel potential that represents the integrated parallel electric field along a magnetic field line. The acceleration and trapping of electrons by such a parallel potential lead to the typical flat-top electron distribution observed in reconnection (Egedal et al., 2015). In our event, the parallel electric field points outward from the X line, yielding a positive parallel potential. The parallel potential is estimated to be 30 V, based on Liouville mapping of electron distributions from the background electrons to the energized electrons in

the reconnection region. The value of the estimated parallel potential is comparable to that in another magnetosheath reconnection event (E. Eriksson et al., 2018). This potential causes substantial electron acceleration and trapping, associated with field-aligned bidirectional beams, increased electron pressure, and temperature anisotropy $T_{e\parallel} > T_{e\perp}$ observed in the reconnection region. Note that the maximum energy for the field-aligned bidirectional distribution is approximately 400 eV, larger than the estimated parallel potential. Therefore, magnetic trapping due to the mirror force (Q. M. Lu et al., 2010; R. S. Wang et al., 2010) also works therein. The increased electron density suggests that parallel electric field trapping in our event plays a dominant role than the magnetic well (Egedal et al., 2008; Nan et al., 2022).

Both electrons outside and inside the reconnection region exhibit typical flat-top distributions, with maximum flat-top energy of 40 and 70 eV, respectively. It is evident that the parallel potential in the localized reconnection region accelerates the inflowing electrons, leading to an increase in the maximum energy of the flat-top electrons. This acceleration by the parallel potential dominates the increase in the electron PSD for energies below 300 eV, which is approximately 10 times the background electron temperature. As a result, the electron temperature rises from 30 to 50 eV. For electrons with energies greater than 300 eV, the PSD exceeds that predicted by parallel potential acceleration alone, suggesting that these electrons are further accelerated by other mechanisms. This mechanism appears to be more effective for high-energy electron acceleration. Additionally, some processes should be involved within the current sheet to scatter the electrons to cause an increase in the electron perpendicular PSD. One possibility is that electrons become stochastic near the X line, where their Larmor radius is comparable to the curvature radius of the magnetic field (X. R. Fu et al., 2006; R. S. Wang et al., 2010). This potential pitch-angle scattering process causes a slight increase in the electron perpendicular temperature from 30 to 35 eV, and results in an isotropic distribution for electrons with energies greater than 300 eV.

Strong electric fields are frequently observed in magnetic reconnection events, such as those in Earth's magnetotail (Ergun et al., 2022; Genestreti et al., 2018; Qi et al., 2024). Magnetotail reconnection typically causes large-scale magnetic field reconfiguration and generates strong turbulence, which drives small-scale reconnection (Ergun et al., 2022; Qi et al., 2024; Zhou et al., 2021). Ergun et al. (2018) reported observations of extraordinarily large-amplitude parallel electric fields (>100 mV/m) and associated energy dissipation in a turbulent magnetotail reconnection region. These parallel electric field events cause large potentials (>1 kV) along the magnetic field and accelerate electrons, which is similar to the acceleration process observed in our event. Large-amplitude electric field structures in turbulence driven by magnetotail reconnection cause significant energy conversion from the magnetic field to the particles. This conversion can energize ions and electrons trapped in turbulence-generated structures to hundreds of keV (Ergun et al., 2020a, 2020b; Li et al., 2022). Despite differences in the energy sources driving turbulence between the magnetotail reconnection region and the magnetosheath, the strong electric fields and associated energy conversion processes in turbulence-driven reconnection appear remarkably similar. This similarity implies that such processes may also operate in other astrophysical environments, such as supernova shells, and could potentially explain cosmic-ray acceleration resulting from turbulent magnetic reconnection (Ergun et al., 2020a).

The electron energization by a localized acceleration potential in the turbulent magnetosheath is informative. Previous studies have shown that some resonant mechanisms, such as Landau or cyclotron resonant damping (He et al., 2015; Howes et al., 2011; Leamon et al., 1998), non-resonant mechanisms like stochastic heating (Chandran et al., 2013; Voitenko & Goossens, 2004), and magnetic reconnection (Loureiro & Boldyrev, 2017; Retinò et al., 2007) can cause significant dissipation and heating in the turbulence. In the magnetosheath downstream of the quasi-parallel shock, turbulence is strong, and numerous small-scale current sheets are formed (Retinò et al., 2007; Schwartz et al., 2021; S. M. Wang, Lu, et al., 2024; Xu et al., 2023). Our study demonstrates that the parallel electric field and the resulting acceleration potential within such a localized reconnecting current sheet can directly accelerate electrons, generating field-aligned bidirectional beams and flat-top electron distributions, accompanied by significant parallel electron heating. The cumulative effect of this mechanism in a turbulent environment which is filled with many current sheets can be substantial.

Data Availability Statement

The MMS data used in this work are available at the MMS data center (<https://lasp.colorado.edu/mms/sdc/public/about/browse-wrapper/>).

Acknowledgments

We thank the entire MMS team for providing such excellent and well-calibrated data that permits this study. This work is supported by the National Science Foundation of China (NSFC) grants (42404163, 41922030, 42174181, and 42174187), the Fundamental Research Funds for the Central Universities, the Project funded by China Postdoctoral Science Foundation (2024T170876 and 2023M743356), the Postdoctoral Fellowship Program of CPSF, and the Xiaomi Young Talents Program.

References

- Asano, Y., Nakamura, R., Shinohara, I., Fujimoto, M., Takada, T., Baumjohann, W., et al. (2008). Electron flat-top distributions around the magnetic reconnection region. *Journal of Geophysical Research*, 113(A1). <https://doi.org/10.1029/2007ja012461>
- Bai, S. C., Guo, R. L., Xiao, Y. C., Shi, Q. Q., Yao, Z. H., Pu, Z. Y., et al. (2025). Spontaneously generated flux ropes in 3-D magnetic reconnection. *Journal of Geophysical Research: Space Physics*, 130(1), e2024JA033461. <https://doi.org/10.1029/2024JA033461>
- Bai, S. C., Shi, Q. Q., Zong, Q. G., Wang, X. G., Tian, A. M., Degeling, A. W., et al. (2019). Electron dispersion and parallel electron beam observed near the separatrix. *Journal of Geophysical Research: Space Physics*, 124(9), 7494–7504. <https://doi.org/10.1029/2019ja026836>
- Birn, J., & Hesse, M. (2014). Forced reconnection in the near magnetotail: Onset and energy conversion in PIC and MHD simulations. *Journal of Geophysical Research: Space Physics*, 119(1), 290–309. <https://doi.org/10.1002/2013ja019354>
- Bruno, R., & Carbone, V. (2013). The solar wind as a turbulence laboratory. *Living Reviews in Solar Physics*, 10(2), 7. <https://doi.org/10.12942/lrsp-2013-2>
- Burch, J. L., Moore, T. E., Torbert, R. B., & Giles, B. L. (2016). Magnetospheric multiscale overview and science objectives. *Space Science Reviews*, 199(1–4), 5–21. <https://doi.org/10.1007/s11214-015-0164-9>
- Burch, J. L., Torbert, R. B., Phan, T. D., Chen, L. J., Moore, T. E., Ergun, R. E., et al. (2016). Electron-scale measurements of magnetic reconnection in space. *Science*, 352(6290). <https://doi.org/10.1126/science.aaf2939>
- Burch, J. L., Webster, J. M., Hesse, M., Genestreti, K. J., Denton, R. E., Phan, T. D., et al. (2020). Electron inflow velocities and reconnection rates at Earth's magnetopause and magnetosheath. *Geophysical Research Letters*, 47(17), e2020GL089082. <https://doi.org/10.1029/2020GL089082>
- Chandran, B. D. G., Verscharen, D., Quataert, E., Kasper, J. C., Isenberg, P. A., & Bourouaine, S. (2013). Stochastic heating, differential flow, and the alpha-to-proton temperature ratio in the solar wind. *Astrophys J*, 776(1). <https://doi.org/10.1088/0004-637x/776/1/45>
- Chang, C., Huang, K., Lu, Q. M., Lu, S., Yu, X. C., Wang, R. S., et al. (2022). Electrostatic solitary waves and electron-beam instabilities in the separatrix region of magnetic reconnection. *The Astrophysical Journal*, 933(1). <https://doi.org/10.3847/1538-4357/ac738d>
- Chasapis, A., Retinò, A., Sahraoui, F., Vaivads, A., Khotyaintsev, Y. V., Sundkvist, D., et al. (2015). Thin current sheets and associated electron heating in turbulent space plasma. *The Astrophysical Journal Letters*, 804(1). <https://doi.org/10.1088/2041-8205/804/1/L1>
- Chen, X. H., Fu, H. S., Liu, C. M., Cao, D., Wang, Z., Dunlop, M. W., et al. (2018). Magnetic nulls in the reconnection driven by turbulence. *The Astrophysical Journal*, 852(1). <https://doi.org/10.3847/1538-4357/aa9991>
- Dahlin, J. T., Drake, J. F., & Swisdak, M. (2016). Parallel electric fields are inefficient drivers of energetic electrons in magnetic reconnection. *Physics of Plasmas*, 23(12). <https://doi.org/10.1063/1.4972082>
- Daughton, W., Roytershteyn, V., Karimabadi, H., Yin, L., Albright, B. J., Bergen, B., & Bowers, K. J. (2011). Role of electron physics in the development of turbulent magnetic reconnection in collisionless plasmas. *Nature Physics*, 7(7), 539–542. <https://doi.org/10.1038/Nphys1965>
- Dmitruk, P., Matthaeus, W. H., & Seenu, N. (2004). Test particle energization by current sheets and nonuniform fields in magnetohydrodynamic turbulence. *The Astrophysical Journal*, 617(1), 667–679. <https://doi.org/10.1086/425301>
- Drake, J. F., Shay, M. A., Thongthai, W., & Swisdak, M. (2005). Production of energetic electrons during magnetic reconnection. *Physical Review Letters*, 94(9). <https://doi.org/10.1103/PhysRevLett.94.095001>
- Drake, J. F., Swisdak, M., Cattell, C., Shay, M. A., Rogers, B. N., & Zeiler, A. (2003). Formation of electron holes and particle energization during magnetic reconnection. *Science*, 299(5608), 873–877. <https://doi.org/10.1126/science.1080333>
- Dunlop, M. W., Balogh, A., Glassmeier, K. H., & Robert, P. (2002). Four-point cluster application of magnetic field analysis tools: The curlometer. *Journal of Geophysical Research*, 107(A11). <https://doi.org/10.1029/2001ja005088>
- Egedal, J., Daughton, W., Le, A., & Borg, A. L. (2015). Double layer electric fields aiding the production of energetic flat-top distributions and superthermal electrons within magnetic reconnection exhausts. *Physics of Plasmas*, 22(10). <https://doi.org/10.1063/1.4933055>
- Egedal, J., Fox, W., Katz, N., Porkolab, M., Oieroset, M., Lin, R. P., et al. (2008). Evidence and theory for trapped electrons in guide field magnetotail reconnection. *Journal of Geophysical Research*, 113(A12). <https://doi.org/10.1029/2008ja013520>
- Egedal, J., Lê, A., Zhu, Y., Daughton, W., Oieroset, M., Phan, T., et al. (2010). Cause of super-thermal electron heating during magnetotail reconnection. *Geophysical Research Letters*, 37. <https://doi.org/10.1029/2010gl043487>
- Ergun, R. E., Ahmadi, N., Kromyda, L., Schwartz, S. J., Chasapis, A., Hoilijoki, S., et al. (2020a). Particle acceleration in strong turbulence in the Earth's magnetotail. *The Astrophysical Journal*, 898(2), 153. <https://doi.org/10.3847/1538-4357/ab9ab5>
- Ergun, R. E., Ahmadi, N., Kromyda, L., Schwartz, S. J., Chasapis, A., Hoilijoki, S., et al. (2020b). Observations of particle acceleration in magnetic reconnection-driven turbulence. *The Astrophysical Journal*, 898(2), 154. <https://doi.org/10.3847/1538-4357/ab9ab6>
- Ergun, R. E., Goodrich, K. A., Wilder, F. D., Ahmadi, N., Holmes, J. C., Eriksson, S., et al. (2018). Magnetic reconnection, turbulence, and particle acceleration: Observations in the Earth's magnetotail. *Geophysical Research Letters*, 45(8), 3338–3347. <https://doi.org/10.1002/2018gl076993>
- Ergun, R. E., Holmes, J. C., Goodrich, K. A., Wilder, F. D., Stawarz, J. E., Eriksson, S., et al. (2016). Magnetospheric multiscale observations of large-amplitude, parallel, electrostatic waves associated with magnetic reconnection at the magnetopause. *Geophysical Research Letters*, 43(11), 5626–5634. <https://doi.org/10.1002/2016gl068992>
- Ergun, R. E., Pathak, N., Usanova, M. E., Qi, Y., Vo, T., Burch, J. L., et al. (2022). Observation of magnetic reconnection in a region of strong turbulence. *The Astrophysical Journal Letters*, 935(1), L8. <https://doi.org/10.3847/2041-8213/ac81d4>
- Ergun, R. E., Tucker, S., Westfall, J., Goodrich, K. A., Malaspina, D. M., Summers, D., et al. (2016). The axial double probe and fields signal processing for the MMS mission. *Space Science Reviews*, 199(1–4), 167–188. <https://doi.org/10.1007/s11214-014-0115-x>
- Eriksson, E., Vaivads, A., Graham, D. B., Divin, A., Khotyaintsev, Y. V., Yordanova, E., et al. (2018). Electron energization at a reconnecting magnetosheath current sheet. *Geophysical Research Letters*, 45(16), 8081–8090. <https://doi.org/10.1029/2018gl078660>
- Eriksson, E., Vaivads, A., Graham, D. B., Khotyaintsev, Y. V., Yordanova, E., Hietala, H., et al. (2016). Strong current sheet at a magnetosheath jet: Kinetic structure and electron acceleration. *Journal of Geophysical Research: Space Physics*, 121(10), 9608–9618. <https://doi.org/10.1002/2016ja023146>
- Eriksson, S., Wilder, F. D., Ergun, R. E., Schwartz, S. J., Cassak, P. A., Burch, J. L., et al. (2016). Magnetospheric multiscale observations of the electron diffusion region of large guide field magnetic reconnection. *Physical Review Letters*, 117(1). <https://doi.org/10.1103/PhysRevLett.117.015001>
- Feldman, W., Anderson, R., Bame, S., Gary, S., Gosling, J., McComas, D., et al. (1983). Electron velocity distributions near the Earth's bow shock. *Journal of Geophysical Research*, 88(A1), 96–110.
- Fox, W., Wilder, F. D., Eriksson, S., Jara-Almonte, J., Pucci, F., Yoo, J., et al. (2018). Energy conversion by parallel electric fields during guide field reconnection in scaled laboratory and space experiments. *Geophysical Research Letters*, 45(23), 12677–12684. <https://doi.org/10.1029/2018gl079883>

- Fu, H. S., Vaivads, A., Khotyaintsev, Y. V., Andre, M., Cao, J. B., Olshevsky, V., et al. (2017). Intermittent energy dissipation by turbulent reconnection. *Geophysical Research Letters*, 44(1), 37–43. <https://doi.org/10.1002/2016gl017187>
- Fu, X. R., Lu, Q. M., & Wang, S. (2006). The process of electron acceleration during collisionless magnetic reconnection. *Physics of Plasmas*, 13(1). <https://doi.org/10.1063/1.2164808>
- Fu, X. S., Zhong, Z. H., Zhou, M., Ma, W. Q., Pang, Y., Song, L. J., et al. (2024). Electron acceleration via secondary reconnection in the separatrix region of magnetopause reconnection. *Geophysical Research Letters*, 51(17). <https://doi.org/10.1029/2024GL110152>
- Genestreti, K. J., Nakamura, T. K. M., Nakamura, R., Denton, R. E., Torbert, R. B., Burch, J. L., et al. (2018). How accurately can we measure the reconnection rate E_M for the MMS diffusion region event of 11 July 2017? *Journal of Geophysical Research: Space Physics*, 123(11), 9130–9149. <https://doi.org/10.1029/2018ja025711>
- Graham, D. B., Cozzani, G., Khotyaintsev, Y. V., Wilder, V. D., Holmes, J. C., Nakamura, T. K. M., et al. (2025). The role of kinetic instabilities and waves in collisionless magnetic reconnection. *Space Science Reviews*, 221(1), 20. <https://doi.org/10.1007/s11214-024-01133-7>
- Graham, D. B., Khotyaintsev, Y. V., André, M., Vaivads, A., Chasapis, A., Matthaeus, W. H., et al. (2021). Non-maxwellianity of electron distributions near Earth's magnetopause. *Journal of Geophysical Research: Space Physics*, 126(10). <https://doi.org/10.1029/2021JA029260>
- Guo, A., Lu, Q. M., Lu, S., Wang, S. M., & Wang, R. S. (2023). Properties of electron-scale magnetic reconnection at a quasi-perpendicular shock. *The Astrophysical Journal*, 955(1). <https://doi.org/10.3847/1538-4357/acec48>
- He, J. S., Wang, L. H., Tu, C. Y., Marsch, E., & Zong, Q. G. (2015). Evidence of Landau and cyclotron resonance between protons and kinetic waves in solar wind turbulence. *The Astrophysical Journal Letters*, 800(2). <https://doi.org/10.1088/2041-8205/800/2/L31>
- Howes, G. G., TenBarge, J. M., Dorland, W., Quataert, E., Schekochihin, A. A., Numata, R., & Tatsuno, T. (2011). Gyrokinetic simulations of solar wind turbulence from ion to electron scales. *Physical Review Letters*, 107(3). <https://doi.org/10.1103/PhysRevLett.107.035004>
- Huang, C., Lu, Q. M., & Wang, S. (2010). The mechanisms of electron acceleration in antiparallel and guide field magnetic reconnection. *Physics of Plasmas*, 17(7). <https://doi.org/10.1063/1.3457930>
- Huang, S. Y., Xiong, Q. Y., Song, L. F., Nan, J., Yuan, Z. G., Jiang, K., et al. (2021). Electron-only reconnection in an ion-scale current sheet at the magnetopause. *The Astrophysical Journal*, 922(1). <https://doi.org/10.3847/1538-4357/ac2668>
- Karimabadi, H., Roytershteyn, V., Vu, H. X., Omelchenko, Y. A., Scudder, J., Daughton, W., et al. (2014). The link between shocks, turbulence, and magnetic reconnection in collisionless plasmas. *Physics of Plasmas*, 21(6). <https://doi.org/10.1063/1.4882875>
- Lapenta, G., Markidis, S., Divin, A., Goldman, M., & Newman, D. (2010). Scales of guide field reconnection at the hydrogen mass ratio. *Physics of Plasmas*, 17(8). <https://doi.org/10.1063/1.3467503>
- Leamon, R. J., Matthaeus, W. H., Smith, C. W., & Wong, H. K. (1998). Contribution of cyclotron-resonant damping to kinetic dissipation of interplanetary turbulence. *The Astrophysical Journal*, 507(2), L181–L184. <https://doi.org/10.1086/311698>
- Li, X. M., Wang, R. S., Lu, Q. M., Russell, C. T., Lu, S., Cohen, I. J., et al. (2022). Three-dimensional network of filamentary currents and super-thermal electrons during magnetotail magnetic reconnection. *Nature Communications*, 13(1), 3241. <https://doi.org/10.1038/s41467-022-31025-9>
- Lindqvist, P. A., Olsson, G., Torbert, R. B., King, B., Granoff, M., Rau, D., et al. (2016). The spin-plane double probe electric field instrument for MMS. *Space Science Reviews*, 199(1–4), 137–165. <https://doi.org/10.1007/s11214-014-0116-9>
- Liu, D. K., Lu, S., Lu, Q. M., Ding, W. X., & Wang, S. (2020). Spontaneous onset of collisionless magnetic reconnection on an electron scale. *The Astrophysical Journal Letters*, 890(2). <https://doi.org/10.3847/2041-8213/ab72fe>
- Liu, Y. H., Hesse, M., Guo, F., Daughton, W., Li, H., Cassak, P. A., & Shay, M. A. (2017). Why does steady-state magnetic reconnection have a maximum local rate of order 0.1? *Physical Review Letters*, 118(8), 085101. <https://doi.org/10.1103/PhysRevLett.118.085101>
- Loureiro, N. F., & Boldyrev, S. (2017). Role of magnetic reconnection in magnetohydrodynamic turbulence. *Physical Review Letters*, 118(24). <https://doi.org/10.1103/PhysRevLett.118.245101>
- Lu, Q., Shu, Y., Chang, C., Lu, S., & Wang, R. (2025). The rate of magnetic reconnection in non-steady state. *Science Bulletin*. <https://doi.org/10.1016/j.scib.2025.06.014>
- Lu, Q. M., Guo, A., Yang, Z. W., Wang, R. S., Lu, S., Chen, R., & Gao, X. L. (2024). Upstream plasma waves and downstream magnetic reconnection at a reforming quasi-parallel shock. *The Astrophysical Journal*, 964(1). <https://doi.org/10.3847/1538-4357/ad2456>
- Lu, Q. M., Huang, C., Xie, J. L., Wang, R. S., Wu, M. Y., Vaivads, A., & Wang, S. (2010). Features of separatrix regions in magnetic reconnection: Comparison of 2-D particle-in-cell simulations and cluster observations. *Journal of Geophysical Research*, 115. <https://doi.org/10.1029/2010ja015713>
- Lu, Q. M., Wang, H. Y., Wang, X. Y., Lu, S., Wang, R. S., Gao, X. L., & Wang, S. (2020). Turbulence-driven magnetic reconnection in the magnetosheath downstream of a quasi-parallel shock: A three-dimensional global hybrid simulation. *Geophysical Research Letters*, 47(1). <https://doi.org/10.1029/2019GL085661>
- Lu, S., Angelopoulos, V., Pritchett, P. L., Nan, J., Huang, K., Tao, X., et al. (2021). Electrodynamics contributions to the Hall- and parallel electric fields in collisionless magnetic reconnection. *Journal of Geophysical Research: Space Physics*, 126(11). <https://doi.org/10.1029/2021JA029550>
- Lu, S., Wang, R. S., Lu, Q. M., Angelopoulos, V., Nakamura, R., Artemyev, A. V., et al. (2020). Magnetotail reconnection onset caused by electron kinetics with a strong external driver. *Nature Communications*, 11(1). <https://doi.org/10.1038/s41467-020-18787-w>
- Mozar, F. S., & Pritchett, P. L. (2010). Spatial, temporal, and amplitude characteristics of parallel electric fields associated with subsolar magnetic field reconnection. *Journal of Geophysical Research*, 115. <https://doi.org/10.1029/2009ja014718>
- Nan, J., Huang, K., Lu, Q. M., Lu, S., Wang, R. S., Xie, J. L., et al. (2022). Formation of the electron inflow along the separatrices during collisionless magnetic reconnection. *Journal of Geophysical Research: Space Physics*, 127(5). <https://doi.org/10.1029/2021JA029996>
- Newman, D. L., Goldman, M. V., Ergun, R. E., & Mangeney, A. (2001). Formation of double layers and electron holes in a current-driven space plasma. *Physical Review Letters*, 87(25). <https://doi.org/10.1103/PhysRevLett.87.255001>
- Oieroset, M., Phan, T. D., Drake, J. F., Eastwood, J. P., Fuselier, S. A., Strangeway, R. J., et al. (2019). Reconnection with magnetic flux pileup at the interface of converging jets at the magnetopause. *Geophysical Research Letters*, 46(4), 1937–1946. <https://doi.org/10.1029/2018gl080994>
- Phan, T. D., Eastwood, J. P., Shay, M. A., Drake, J. F., Sonnerup, B. U. Ö., Fujimoto, M., et al. (2018). Electron magnetic reconnection without ion coupling in Earth's turbulent magnetosheath. *Nature*, 557(7704), 202. <https://doi.org/10.1038/s41586-018-0091-5>
- Plaschke, F., Karlsson, T., Hietala, H., Archer, M., Vörös, Z., Nakamura, R., et al. (2017). Magnetosheath high-speed jets: Internal structure and interaction with ambient plasma. *Journal of Geophysical Research: Space Physics*, 122(10), 10157–10175. <https://doi.org/10.1002/2017ja024471>
- Pollock, C., Moore, T., Jacques, A., Burch, J., Gliese, U., Saito, Y., et al. (2016). Fast plasma investigation for magnetospheric multiscale. *Space Science Reviews*, 199(1–4), 331–406. <https://doi.org/10.1007/s11214-016-0245-4>

- Pritchard, K. R., Burch, J. L., Fuselier, S. A., Genestreti, K. J., Denton, R. E., Webster, J. M., & Broll, J. M. (2023). Reconnection rates at the Earth's magnetopause and in the magnetosheath. *Journal of Geophysical Research: Space Physics*, 128(9), e2023JA031475. <https://doi.org/10.1029/2023JA031475>
- Pritchard, K. R., Burch, J. L., Fuselier, S. A., Webster, J. M., Torbert, R. B., Argall, M. R., et al. (2019). Energy conversion and electron acceleration in the magnetopause reconnection diffusion region. *Geophysical Research Letters*, 46(17–18), 10274–10282. <https://doi.org/10.1029/2019gl084636>
- Pritchett, P. L. (2001). Collisionless magnetic reconnection in a three-dimensional open system. *Journal of Geophysical Research*, 106(A11), 25961–25977. <https://doi.org/10.1029/2001ja000016>
- Pritchett, P. L., & Coroniti, F. V. (2004). Three-dimensional collisionless magnetic reconnection in the presence of a guide field. *Journal of Geophysical Research*, 109(A1). <https://doi.org/10.1029/2003ja009999>
- Qi, Y., Ergun, R., Pathak, N., Phan, T. D., Burch, J. L., Chasapis, A., et al. (2024). Investigation of a magnetic reconnection event with extraordinarily high particle energization in magnetotail turbulence. *The Astrophysical Journal Letters*, 962(2), L39. <https://doi.org/10.3847/2041-8213/ad24eb>
- Retinò, A., Sundkvist, D., Vaivads, A., Mozer, F., Andre, M., & Owen, C. J. (2007). In-situ evidence of magnetic reconnection in turbulent plasma. *Nature Physics*, 3(4), 235–238. <https://doi.org/10.1038/nphys574>
- Russell, C. T., Anderson, B. J., Baumjohann, W., Bromund, K. R., Dearborn, D., Fischer, D., et al. (2016). The magnetospheric multiscale magnetometers. *Space Science Reviews*, 199(1–4), 189–256. <https://doi.org/10.1007/s11214-014-0057-3>
- Schwartz, S. J., Kucharek, H., Farrugia, C. J., Trattner, K., Gingell, I., Ergun, R. E., et al. (2021). Energy conversion within current sheets in the Earth's quasi-parallel magnetosheath. *Geophysical Research Letters*, 48(4). <https://doi.org/10.1029/2020GL091859>
- Scudder, J. D. (1995). A review of the physics of electron heating at collisionless shocks. *Advances in Space Research*, 15(8–9), 181–223.
- Shay, M. A., Phan, T. D., Haggerty, C. C., Fujimoto, M., Drake, J. F., Malakit, K., et al. (2016). Kinetic signatures of the region surrounding the X line in asymmetric (magnetopause) reconnection. *Geophysical Research Letters*, 43(9), 4145–4154. <https://doi.org/10.1002/2016gl069034>
- Shi, Q. Q., Shen, C., Dunlop, M. W., Pu, Z. Y., Zong, Q. G., Liu, Z. X., et al. (2006). Motion of observed structures calculated from multi-point magnetic field measurements: Application to cluster. *Geophysical Research Letters*, 33(8), L08109. <https://doi.org/10.1029/2005gl025073>
- Shi, Q. Q., Shen, C., Pu, Z. Y., Dunlop, M. W., Zong, Q. G., Zhang, H., et al. (2005). Dimensional analysis of observed structures using multipoint magnetic field measurements: Application to cluster. *Geophysical Research Letters*, 32(12), L12105. <https://doi.org/10.1029/2005gl022454>
- Sonnerup, B. U., & Cahill, L. J. (1967). Magnetopause structure and attitude from explorer 12 observations. *Journal of Geophysical Research*, 72(1), 171. <https://doi.org/10.1029/JZ072i001p00171>
- Stawarz, J. E., Eastwood, J. P., Phan, T. D., Gingell, I. L., Pykurel, P. S., Shay, M. A., et al. (2022). Turbulence-driven magnetic reconnection and the magnetic correlation length: Observations from magnetospheric multiscale in Earth's magnetosheath. *Physics of Plasmas*, 29(1). <https://doi.org/10.1063/5.0071106>
- Steinva, K., Khotyaintsev, Y., Graham, D. B., Vaivads, A., André, M., & Russell, C. T. (2021). Large amplitude electrostatic proton plasma frequency waves in the magnetospheric separatrix and outflow regions during magnetic reconnection. *Geophysical Research Letters*, 48(5), e2020GL090286. <https://doi.org/10.1029/2020GL090286>
- Sundkvist, D., Retinò, A., Vaivads, A., & Bale, S. D. (2007). Dissipation in turbulent plasma due to reconnection in thin current sheets. *Physical Review Letters*, 99(2). <https://doi.org/10.1103/PhysRevLett.99.025004>
- Voitenko, Y., & Goossens, M. (2004). Cross-field heating of coronal ions by low-frequency kinetic Alfvén waves. *The Astrophysical Journal*, 605(2), L149–L152. <https://doi.org/10.1086/420927>
- Vörös, Z., Yordanova, E., Varsani, A., Genestreti, K. J., Khotyaintsev, Y. V., Li, W., et al. (2017). MMS observation of magnetic reconnection in the turbulent magnetosheath. *Journal of Geophysical Research: Space Physics*, 122(11), 11442–11467. <https://doi.org/10.1002/2017ja024535>
- Vörös, Z., Yordanova, E., Echim, M. M., Consolini, G., & Narita, Y. (2016). Turbulence-generated proton-scale structures in the terrestrial magnetosheath. *The Astrophysical Journal Letters*, 819(1). <https://doi.org/10.3847/2041-8205/819/1/L15>
- Wan, M., Matthaeus, W. H., Karimabadi, H., Roytershteyn, V., Shay, M., Wu, P., et al. (2012). Intermittent dissipation at kinetic scales in collisionless plasma turbulence. *Physical Review Letters*, 109(19). <https://doi.org/10.1103/PhysRevLett.109.195001>
- Wang, H. W., Tang, B. B., Li, W. Y., Zhang, Y. C., Graham, D. B., Khotyaintsev, Y. V., et al. (2023). Electron dynamics in the electron current sheet during strong guide-field reconnection. *Geophysical Research Letters*, 50(10). <https://doi.org/10.1029/2023GL103046>
- Wang, R. S., Du, A. M., Nakamura, R., Lu, Q. M., Khotyaintsev, Y. V., Volwerk, M., et al. (2013). Observation of multiple sub-cavities adjacent to single separatrix. *Geophysical Research Letters*, 40(11), 2511–2517. <https://doi.org/10.1002/grl.50537>
- Wang, R. S., Lu, Q. M., Huang, C., & Wang, S. (2010). Multispacecraft observation of electron pitch angle distributions in magnetotail reconnection. *Journal of Geophysical Research*, 115. <https://doi.org/10.1029/2009ja014553>
- Wang, R. S., Lu, Q. M., Khotyaintsev, Y. V., Volwerk, M., Du, A. M., Nakamura, R., et al. (2014). Observation of double layer in the separatrix region during magnetic reconnection. *Geophysical Research Letters*, 41(14), 4851–4858. <https://doi.org/10.1002/2014gl061157>
- Wang, R. S., Nakamura, R., Lu, Q. M., Baumjohann, W., Ergun, R. E., Burch, J. L., et al. (2017). Electron-scale quadrants of the hall magnetic field observed by the magnetospheric multiscale spacecraft during asymmetric reconnection. *Physical Review Letters*, 118(17). <https://doi.org/10.1103/PhysRevLett.118.175101>
- Wang, S., Chen, L. J., Bessho, N., Hesse, M., Yoo, J., Yamada, M., et al. (2018). Energy conversion and partition in the asymmetric reconnection diffusion region. *Journal of Geophysical Research: Space Physics*, 123(10), 8185–8205. <https://doi.org/10.1029/2018ja025519>
- Wang, S. M., Lu, S., Lu, Q. M., Wang, R. S., Ren, J. Y., Gao, X. L., & Guo, J. (2024). Origin of reconnecting current sheets in shocked turbulent plasma. *Science Advances*, 10(33), eado4639. <https://doi.org/10.1126/sciadv.ad04639>
- Wang, S. M., Wang, R. S., Huang, K., & Guo, J. (2024). A bifurcated reconnecting current sheet in the turbulent magnetosheath. *Magnetochemistry*, 10(11). <https://doi.org/10.3390/magnetochemistry10110089>
- Wang, S. M., Wang, R. S., Lu, Q. M., Burch, J. L., & Wang, S. (2021). Energy dissipation via magnetic reconnection within the coherent structures of the magnetosheath turbulence. *Journal of Geophysical Research: Space Physics*, 126(4). <https://doi.org/10.1029/2020JA028860>
- Wang, S. M., Wang, R. S., Lu, Q. M., Russell, C. T., Ergun, R. E., & Wang, S. (2021). Large-scale parallel electric field collocated in an extended electron diffusion region during the magnetosheath magnetic reconnection. *Geophysical Research Letters*, 48(23). <https://doi.org/10.1029/2021GL094879>
- Wetherton, B. A., Egedal, J., Le, A., & Daughton, W. (2022). Generation of a strong parallel electric field and embedded electron jet in the exhaust of moderate guide field reconnection. *Geophysical Research Letters*, 49(14). <https://doi.org/10.1029/2022GL098907>
- Wilder, F. D., Ergun, R. E., Burch, J. L., Ahmadi, N., Eriksson, S., Phan, T. D., et al. (2018). The role of the parallel electric field in electron-scale dissipation at reconnecting currents in the magnetosheath. *Journal of Geophysical Research: Space Physics*, 123(8), 6533–6547. <https://doi.org/10.1029/2018ja025529>

- Wilder, F. D., Ergun, R. E., Eriksson, S., Phan, T. D., Burch, J. L., Ahmadi, N., et al. (2017). Multipoint measurements of the electron jet of symmetric magnetic reconnection with a moderate guide field. *Physical Review Letters*, 118(26). <https://doi.org/10.1103/PhysRevLett.118.265101>
- Wilder, F. D., Ergun, R. E., Goodrich, K. A., Goldman, M. V., Newman, D. L., Malaspina, D. M., et al. (2016). Observations of whistler mode waves with nonlinear parallel electric fields near the dayside magnetic reconnection separatrix by the magnetospheric multiscale mission. *Geophysical Research Letters*, 43(12), 5909–5917. <https://doi.org/10.1002/2016gl069473>
- Wilder, F. D., Ergun, R. E., Hoilijoki, S., Webster, J. M., Argall, M. R., Ahmadi, N., et al. (2019). A survey of plasma waves appearing near dayside magnetopause electron diffusion region events. *Journal of Geophysical Research: Space Physics*, 124(10), 7837–7849. <https://doi.org/10.1029/2019ja027060>
- Xu, Q. Y., Zhou, M., Ma, W. Q., He, J. S., Huang, S. Y., Zhong, Z. H., et al. (2023). Electron heating in magnetosheath turbulence: Dominant role of the parallel electric field within coherent structures. *Geophysical Research Letters*, 50(6). <https://doi.org/10.1029/2022GL102523>
- Yamada, M., Kulsrud, R., & Ji, H. T. (2010). Magnetic reconnection. *Reviews of Modern Physics*, 82(1), 603–664. <https://doi.org/10.1103/RevModPhys.82.603>
- Yordanova, E., Vörös, Z., Varsani, A., Graham, D. B., Norgren, C., Khotyaintsev, Y. V., et al. (2016). Electron scale structures and magnetic reconnection signatures in the turbulent magnetosheath. *Geophysical Research Letters*, 43(12), 5969–5978. <https://doi.org/10.1002/2016gl069191>
- Yu, X. C., Lu, Q. M., Wang, R. S., Huang, K., Gao, X. L., & Wang, S. (2021). MMS observations of broadband electrostatic waves in electron diffusion region of magnetotail reconnection. *Journal of Geophysical Research: Space Physics*, 126(3). <https://doi.org/10.1029/2020JA028882>
- Zhong, Z. H., Graham, D. B., Khotyaintsev, Y. V., Zhou, M., Le Contel, O., Tang, R. X., & Deng, X. H. (2021). Whistler and broadband electrostatic waves in the multiple X-Line reconnection at the magnetopause. *Geophysical Research Letters*, 48(4), e2020GL091320. <https://doi.org/10.1029/2020GL091320>
- Zhou, M., Man, H. Y., Deng, X. H., Pang, Y., Khotyaintsev, Y., Lapenta, G., et al. (2021). Observations of secondary magnetic reconnection in the turbulent reconnection outflow. *Geophysical Research Letters*, 48(4), e2020GL091215. <https://doi.org/10.1029/2020GL091215>